scientific reports

Check for updates

OPEN

Bone cell differentiation and mineralization in wild-type and osteogenesis imperfecta zebrafish are compromised by per- and poly-fluoroalkyl substances (PFAS)

Francesca Tonelli[1], Cecilia Masiero[1], Carla Aresi[1], Camilla Torriani[2], Simona Villani[2], Guido Premoli[3], Antonio Rossi[1] & Antonella Forlino[1]✉

Perfluorinated compounds (PFAS) are well recognized toxic pollutants for humans, but if their effect is equally harmful for healthy and fragile people is unknown. Addressing this question represents a need for ensuring global health and wellbeing to all individuals in a world facing the progressive increase of aging and aging related diseases. This study aimed to evaluate the impact of perfluorooctane sulfonate (PFOS), perfluorooctanoic acid (PFOA) and perfluorohexanoic acid (PFHxA) exposure on development and skeletal phenotype using the osteogenesis imperfecta (OI) zebrafish model *Chihuahua* (*Chi/+*), carrying a dominant glycine substitution in the α1 chain of collagen I and their wild-type (WT) littermates. To this purpose *Chi/+* and WT zebrafish expressing the green fluorescent protein under the early osteoblast marker *osterix* were exposed from 1 to 6 days post fertilization to 0.36, 1.5 and 3.0 mg/L PFOS, 0.005 and 0.5 mg/L PFOA and 0.01, 0.48 and 16.0 mg/L PFHxA, and their development and skeletal phenotype investigated. Morphometric measurements, confocal microscopy evaluation of operculum area delimited by the fluorescent preosteoblasts and mineral deposition analysis following alizarin red staining were employed. PFOS and the highest concentration of PFHxA significantly impaired standard length in both genotypes. Osteoblast differentiation was significantly compromised by PFOS and by PFOA only in *Chi/+*. Limited to WT exposed to PFOA a reduced mineralization was also observed. No effect was detected after PFHxA exposure. Apoptosis was only activated by PFOA, specifically in *Chi/+* mutant operculum osteoblasts. Interestingly, an altered lipid distribution in both WT and mutant fish was revealed after exposure to both pollutants. In conclusion, our data demonstrate that PFAS impair operculum development mainly compromising cell differentiation in mutant fish whereas alter lipid hepatic distribution in both genotypes with a more severe effect on *Chi/+* preosteoblast survival. These results represent a first warning sign of the negative impact of PFAS exposure in presence of genetically determined skeletal fragility.

Keywords Per- and poly-fluoroalkyl substances, Bone differentiation, Mineralization, Osteogenesis imperfecta, Zebrafish

Per- and poly-fluoroalkyl substances (PFAS) are synthetic fluorinated compounds composed of a carbon backbone of variable length in which each hydrogen atom is substituted by fluorine[1]. They have been widely used in commercial and industrial products like food packaging, cosmetics, waterproof and stain-proof textiles, firefighting foams and pesticides due to their chemical inertness, their thermal stability and their hydrophobicity as well as lipophobicity[1]. The two most widely studied PFAS, namely perfluorooctane sulfonate (PFOS) and perfluorooctanoic acid (PFOA), have been in production since 1950s even if only from 1990 their presence was detected in both environment and in living organisms on a global scale. Due to their half-life, 4 years for PFOS and 2–3 years for PFOA, which make them persistent in the environment and because of their adverse

[1]Department of Molecular Medicine, Biochemistry Unit, University of Pavia, Via Taramelli 3B, 27100 Pavia, Italy. [2]Department of Public Health and Experimental and Forensic Medicine, Unit of Biostatistics and Clinical Epidemiology, University of Pavia, 27100 Pavia, Italy. [3]LabAnalysis Group, Casanova Lonati, 27041 Pavia, Italy. ✉email: aforlino@unipv.it

effects on human health, these molecules have been added in 2008 during the Stockholm Convention to the list of Persistent Organic Pollutants (POPs). A regulated use of PFAS is required since they can potentially affect several organs impacting on development, lipid metabolism and endocrine system by inducing carcinogenicity, immunotoxicity, hepatotoxicity and reprotoxicity[1].

US phased out the use of these chemicals in 2016 (https://www.fda.gov/food/chemicals/authorized-uses-pfas-food-contact-applications) while in Europe they are still used although under a stringent legislative oversight (ECHA, European Chemical Agency).

Short-chain PFAS such as perfluorohexanoic acid (PFHxA) have been produced and used as the substitutes of PFOA and PFOS thanks to the relative safety to human beings due to their short half-life ranging from few days to approximately one month[2–4]. Nevertheless, concerns regarding the largely unknown environmental behaviour, hazards, and toxicity of emerging PFAS are quickly rising.

Of note, several epidemiological studies revealed the association between PFAS exposure and reduced bone mass density, confirming that bone is a target tissue for PFAS. Particularly, the effect of PFAS demonstrated during bone development in infancy and childhood could have a strong impact on young adulthood and beyond, with possible public health implications[5]. Furthermore, high level of PFOS was detected in human bone[6].

Skeletal diseases such as osteoporosis and osteoarthritis, that are associated to the increase in average lifespan of developed countries, could be severely worsen by these pollutants compromising the efficiency and sustainability of the national healthcare systems. In this scenario, the environment can have great impact both mitigating or aggravating the course of ageing associated diseases[7]. Understanding the effect that pollutants have on bone homeostasis as well as finding methods to assess and modulate them is of great relevance for improving population quality of life and reducing healthcare costs.

The use of well characterized animal models represents a unique and strategic tool to dissect the effect that environment can have on bone properties in health and disease. Zebrafish became in the last years a powerful model to study bone and bone disorders. Despite appendicular skeleton is definitely different between zebrafish and human, with human limbs originating from endochondral bones, whereas zebrafish paired fins consist of intramembranous bone supported proximally by endochondral radial bones[8], the conservation between teleost and mammals of bone forming and resorbing cells, of their staminal origin and differentiation pathways as well as of the types of ossification processes makes zebrafish an appealing tool for skeletal study[9]. Furthermore, zebrafish endure cranial to caudal spinal load that is originated by swimming forward through water coupled with caudal propulsion and that is somehow comparable to the gravitational load to which humans are subjected allowing deeper investigation of vertebral column defects with respect the most common rodent models.

Furthermore, the easy manipulation starting from early embryonic stages, the embryo transparency and the availability of transgenic lines carrying fluorescent proteins under the control of specific promoters of genes involved in bone differentiation facilitate, in zebrafish, the analysis of skeletal development and bone mineralization from very early stage limiting time and costs[9]. To date, several zebrafish models for skeletal disorders are available including models for the rare heritable disease osteogenesis imperfecta (OI), a prototype for heritable juvenile osteoporosis[10]. OI is a collagen I related disorder associated to synthesis of misfolded collagen affecting both cell homeostasis and extracellular matrix (ECM) assembly and mineralization[11,12]. Here, we use the well characterized OI zebrafish *Chihuahua* (*Chi*/+) to dissect the effect of the PFAS on skeletal health.

The OI zebrafish *Chi*/+ carries a dominant mutation in the α1 chain of collagen I causing the substitution of a glycine with an aspartate in position 574 of the triple helix (Gly574Asp; p.Gly736Asp) and it is characterized by severe skeletal deformities and multiple fractures, reduced bone mineral density and impaired bone mineralization[12]. It is well known that osteoblasts and adipocytes derive from the same mesenchymal precursors and a fine tuned balance exists from this two cell types[13]. An imbalance in favour of adipogenesis was described in OI and interestingly, *Chi*/+ caudal fin regeneration reproduces this typical OI feature, supporting its uniqueness to investigate the osteoblastogenesis-adipogenesis axis[14,15].

In this study the WT and *Chi*/+ zebrafish crossed with the transgenic line Tg*(OlSp7:nlsGFP)zf132* expressing the green fluorescent protein under the early osteoblastic promoter *osterix* were employed to investigate the negative effect of PFAS exposure on healthy and compromised skeleton, respectively. Bone development and mineralization as well as osteoblast differentiation and activity, were analysed using different techniques to elucidate the mechanism behind the impact of pollutants on bone homeostasis.

Materials and methods

Zebrafish maintenance

Wild type (WT) AB zebrafish were obtained by the European Zebrafish Research Center (EZRC) (Germany). The mutant *Chi*/+ carrying the *col1a1a*-G2207A transition causing the α1(I) Gly574Asp (p.Gly736Asp) substitution[16], and the transgenic line Tg*(OlSp7:nlsGFP)zf132* (referred as Sp7:GFP) were used for the study[17]. Zebrafish embryos were kept in petri dishes in embryo water ($NaHCO_3$ 1.2 mM, instant ocean 0.1 g/L, $CaSO_4$ 1.4 mM, methylene blue 0.00002% w/v) at 28 °C until 6 days post fertilization (dpf), then housed in ZebTEC semiclosed recirculation housing system (Techniplast) at 28 °C, pH 7.5 and conductivity 500 µS on a 14/10 light/dark cycle. Sp7:GFP/WT and *Chi*/+ siblings were obtained by in vitro fertilization using WT eggs and Sp7:GFP/*Chi*/+ sperm. For the experiments, larvae were sacrificed by tricaine overdose (0.03% w/v) in zebrafish water after anaesthesia using tricaine 0.016% w/v (3-amino benzoic acidethylester, Merck). Alternation of dry food and brine shrimps was used for adult zebrafish feeding. All the experiments complied the EU Directive 2010/63/EU, were approved by Italian Ministry of Health (260/2020-PR) and performed in accordance with the relevant guidelines and regulations. The study is reported in accordance with ARRIVE guidelines.

Zebrafish larvae exposure to pollutants

WT and *Chi*/+ larvae were exposed to pollutants starting from 1 dpf after mechanical chorion removal. The exposure concentrations were set at 0.36 mg/L, 1.5 mg/L and 3.0 mg/L for heptadecafluorooctanesulfonic acid tetraethylammonium salt (PFOS, Merck, 365289), 0.005 mg/L and 0.5 mg/L for perfluorooctanoic acid (PFOA, Merck, 171468), and at 0.01 mg/L, 0.48 mg/L and 16.0 mg/L for perfluorohexanoic acid (PFHxA, Merck, 43809)[18–20]. Doses higher than the allowed environmental limit concentration accepted by several countries were purposely selected to evaluate the cumulative effect of the molecule in shorter time scale. The selected lower doses correspond to 10 fold the "environmental quality standard" declared in the D.Lgs 172/2015 for monitoring PFAS in internal surface water of Lombardia (Italy). The higher doses were selected on the basis of previous studies performed on zebrafish, in order to alert about a possible increasingly impact of these compounds on skeleton[18–20]. Larvae were placed into six well plates (20–30 per well) and kept at the above mentioned concentrations of the pollutants or in clean water from 1 to 6 dpf by changing half of the water volume every day and sacrificed. The ending time point was selected to evaluated early zebrafish bone mineralization process that is starting at 4 dpf and thus detectable by 6 dpf[9]. Supplementary Table 1 summarizes the comparisons performed throughout the study.

Zebrafish morphometry analysis

Lateral images were acquired using the stereo microscope Leica M165 FC connected to a Leica Flexacam C3 digital camera. Measurements were performed using the Leica Application Suite X (LAS X) software (Leica) as described in[21]. The Standard Length (SL) was measured as the distance from the snout to the posterior tip of the notochord. Larval development was also investigated by evaluating the inflation of the first lobe of the swim bladder[22,23].

Bone staining and imaging

Sp7:GFP/WT and Sp7:GFP/*Chi*/+ larvae were incubated for 2 h at 28 °C with 50 µg/mL Alizarin Red S (ARS) in HEPES 10 mM dissolved in embryo water, according to[24]. Sp7:GFP positive larvae, stained with ARS, were fixed in paraformaldehyde (PFA) 4% w/v in phosphate-buffered saline (PBS) with $CaCl_2$ 0.9 mM and $MgCl_2$ 0.49 mM, pH 7.4 at 4 °C overnight. Then, samples were washed and stored in PBS with $CaCl_2$ 0.9 mM and $MgCl_2$ 0.49 mM, pH 7.4 at 4 °C overnight. Finally, larvae were mounted on slides using Methyl cellulose 3% w/v (Merck). Z stacks of operculum were acquired applying GFP and Rhodamine filters using a Leica DM6B Wide Field microscope. The green area, represented by Sp7:GFP positive osteoblasts, and the red area, indicating the region of mineralized operculum, were measured using ImageJ toolset ZFBONE[25].

RNA extraction

RNA was extracted from a minimum of three pools ($n = 15–20$ larvae per each pool) of 6 dpf controls and PFAS exposed WT and *Chi*/+ larvae using QIAzol Lysis Reagent (Qiagen) according to manufacturer's instructions. DNA free kit DNase Treatment & Removal (Invitrogen) was used to eliminate genomic DNA traces. RNA quantity was determined by NanoDrop spectrophotometer, and its quality by agarose gel 1% w/v electrophoresis in TBE buffer. Reverse-transcription was performed using the High-Capacity cDNA Transcription kit (Applied Biosystems) according to manufacturer's protocol in a final volume of 20 µL. The expression of *runx2a*, *sp7*, *bcl-2a*, *bida*, *pparα*, *ppary* was evaluated by Real time quantitative PCR (RT-qPCR). *βactin* was used as normalizer. RT-qPCR was performed with SYBR Green Master mix (Applied Biosystems) in triplicate in 25 µL final volume using the following cycle: 2 min at 95 °C, 44 cycles of 5 s at 95 °C, 30 s at the 62–68 °C followed by 1 s at 72 °C[26]. The dissociation curve was performed to confirm the specificity of the amplification. The relative expression was calculated using ΔΔCt method. The QuantStudio 3 thermocycler and the QuantStudio Design & Analysis software (Applied Biosystems) were used. Primer sequences are reported in Supplementary Table 2.

Oil red O (ORO) staining

WT and *Chi*/+ larvae were fixed in PFA 4% v/v overnight at 4˚C, washed with PBS, and stained with Oil red O 0.3% (Merck) in 2-propanol 60% v/v for 2 h and then rinsed in PBS as described in[27]. Samples were mounted in Methyl cellulose 3% w/v (Merck) and images were acquired using a Leica DM6B Wide Field microscope at 10X magnification. The intensity of red signal was classified as moderate (1), intermediate (2) or diffuse (3) according to the distribution of lipids. Two operators blinded to the genotype of the fish qualitatively described the level and spreading of lipids for each embryo.

Tunel assay

Apoptosis was evaluated by Click-iT Plus TUNEL Assay (Invitrogen, C10619) according to manufacturer's instructions. Briefly, treated and untreated Sp7:GFP/WT and Sp7:GFP/*Chi*/+ larvae were fixed in PFA 4% v/v overnight at 4˚C, washed with PBS and dehydrated in absolute methanol overnight at − 20 °C. Larvae were then rehydrated and permeabilized for 1 h with proteinase-K, fixed in PFA 4% v/v 15 min at 37 °C and 15 min at RT and then washed in PBT (PBS-Triton X-100 0.1%).

After incubation with Terminal Deoxynucleotidyl Transferase (TdT) reaction cocktail for 1 h at 37 °C larvae were washed in BSA 3% in PBT and incubated with Click-IT reaction cocktail 30 min at RT. Samples were then washed in PBS at 4 °C overnight[28]. Larvae treated with 1 unit of DNAse I (Thermofisher) in 1X reaction buffer for 30 min or without TdT enzyme incubation were used as positive and negative controls, respectively (Supplementary Fig. 1A). Images were acquired using Leica SP8 DLS confocal microscope with a 25X water objective (Leica HC FLUOTAR L VISIR, 25x/0.95NA). 3D rendering of the operculum and a standardized pipeline developed in house allowed the colocalization of Sp7:GFP and TUNEL signals using Arivis Vision 4D 4.1.2 software (Zeiss) (Supplementary Fig. 1D). The number of TUNEL positive signals was also calculated.

PFAS concentration in water

Water of the last 24 h of exposure was collected and the concentrations of PFOS, PFOA and PFHxA were measured by high-performance liquid chromatography (Agilent UPLC 1290 infinity II) -tandem mass spectrometry (Agilent LC-MS 6475) using Luna Omega C18 50*4.6 mm 3.5 µm or equivalent column, according to ASTM D7979-20 method for PFAS determination. Starting from a custom mix at a concentration of 200 mg/L of each PFAS, a calibration line from 0.01 to 10 µg/L was generated by serial dilution. The sample (5 mL) is collected in a polypropylene tube and the total sample is processed in order to limit target analyte loss due to sample manipulation. In order to monitor all the different steps of the analytical procedure the sample, just after collection has been spiked with surrogates. These surrogates are ^{13}C labelled PFAS and most of them have exactly the same chemical structure of the monitored PFAS (Supplementary Table 3). Acceptance criteria regarding the recovery of these labelled surrogates should be within the 70–130 range. Surrogate mix was added at the samples in concentration of 0.1 µg/L. The collected sample, after the surrogate spike, was prepared for injection by diluting 5 ml of the sample with 5 ml of methanol in a PFAS-free plastic bottle; the sample was acidified with acetic acid to reach pH of 3 and the internal standard was added. Individual PFAS were quantified using the internal standards method with recognition of selected transitions and retention time. The instrument's data processing software constructs the calibration line using the response factor average method and provides an analyte result on the sample expressed in µg/L considering the dilution factor applied to each sample.

Statistical analysis

Quantitative variables were expressed as mean ± standard deviation (SD) or median with 25th and 75th percentiles. Qualitative variables were presented as percentages. The effects of different pollutant concentrations and genotype were assessed using a two-way parametric ANOVA. When the interaction between pollutant concentration and genotype was not statistically significant, a stratified analysis by genotype (WT and *Chi*/+) was performed. For these stratified analyses, parametric ANOVA was used unless the assumptions of normality (Shapiro-Wilk test) and homoscedasticity were violated, in which case a non-parametric Kruskal-Wallis test was applied. Significant results from stratified analyses were further analyzed using Dunnet post-hoc test. Bonferroni's correction was applied to adjust for multiple comparisons. Differences in qualitative variables among exposure groups were evaluated using the chi-squared test. When assumptions for the chi-squared test were not met, Fisher's exact test was used. Interactions with genotype were assessed using logistic or multinomial models, followed by stratified analyses within genotypes using Fisher's exact test and post-hoc comparisons. Exploratory analysis on not exposed WT and *Chi*/+ larvae and gene expression data was conducted using the Wilcoxon rank-sum test. A p-value of < 0.05 was considered statistically significant. Statistical analyses were performed using R version 4.4.1.

Results

Water analysis revealed PFAS different in vivo absorption

To determine if the level of absorption of the different pollutants was similar an indirect approach was employed. HPLC-MS analysis of the water collected at the end of exposure was performed. As expected based on the skin permeability of the pollutants[29], a reduced amount of the original concentrations of PFOS (0.36 mg/L, 1.5 mg/L, 3.0 mg/L), PFOA (0.005 mg/L, 0.5 mg/L) and PFHxA (0.01 mg/L, 0.48 mg/L) was found (Table 1). It has to be taken into account that these are indirect measurements and a possible plastic adsorption of PFAS cannot be excluded.

Mineral deposited, but not early osteoblast differentiation is impaired in 6 dpf *Chi*/+

The dominant OI zebrafish *Chihuahua* (*Chi*/+) carrying the mutation Gly574Asp in α1(I) crossed with the transgenic reporter line expressing fluorescent GFP marker under the early osteoblast promoter *osterix* (Sp7), and the WT GFP transgenic littermates (Sp7:GFP/*Chi*/+ and Sp7:GFP/WT, respectively) were used. The operculum is a membranous bone located in the zebrafish cranium and it was chosen for the analyses since it is well-recognized as consistent, robust and rapid drug screening system to evaluate the effect of bone targeting molecules[30]. To evaluate bone cell differentiation the area of the operculum delimited by the GFP preosteoblasts cells was measured, whereas to quantify the mineral area deposited on the bone, a specific dye binding to the Ca^{2+} of the hydroxyapatite crystals, namely alizarin red, was selected. Following alizarin red staining, the Sp7:GFP and the mineralized area of the operculum were evaluated on 6 dpf larvae (Fig. 1A). The operculum area delimited by Sp7:GFP preosteoblasts was similar in WT and *Chi*/+ and no difference in the expression

Pollutant (original concentration)	Corresponding ^{13}C surrogate	Mean concentration in the collected water	Percentage in the water*
PFOS (0.36 mg/L)	M-PFOS-C8	0.115 ± 0.038	32%
PFOS (1.5 mg/L)	M-PFOS-C8	0.433 ± 0.016	29%
PFOA (0.005 mg/L)	M-PFOA-C8	0.0016 ± 0.0002	32%
PFOA (0.5 mg/L)	M-PFOA-C8	0.192 ± 0.026	38%
PFHxA (0.01 mg/L)	M-PFHXA-C5	0.0035 ± 0.002	35%
PFHxA (0.48 mg/L)	M-PFHXA-C5	0.145 ± 0.043	30%

Table 1. Concentrations of PFOS, PFOA and PFHxA detected by HPLC-MS. *Referred to the original administered concentration.

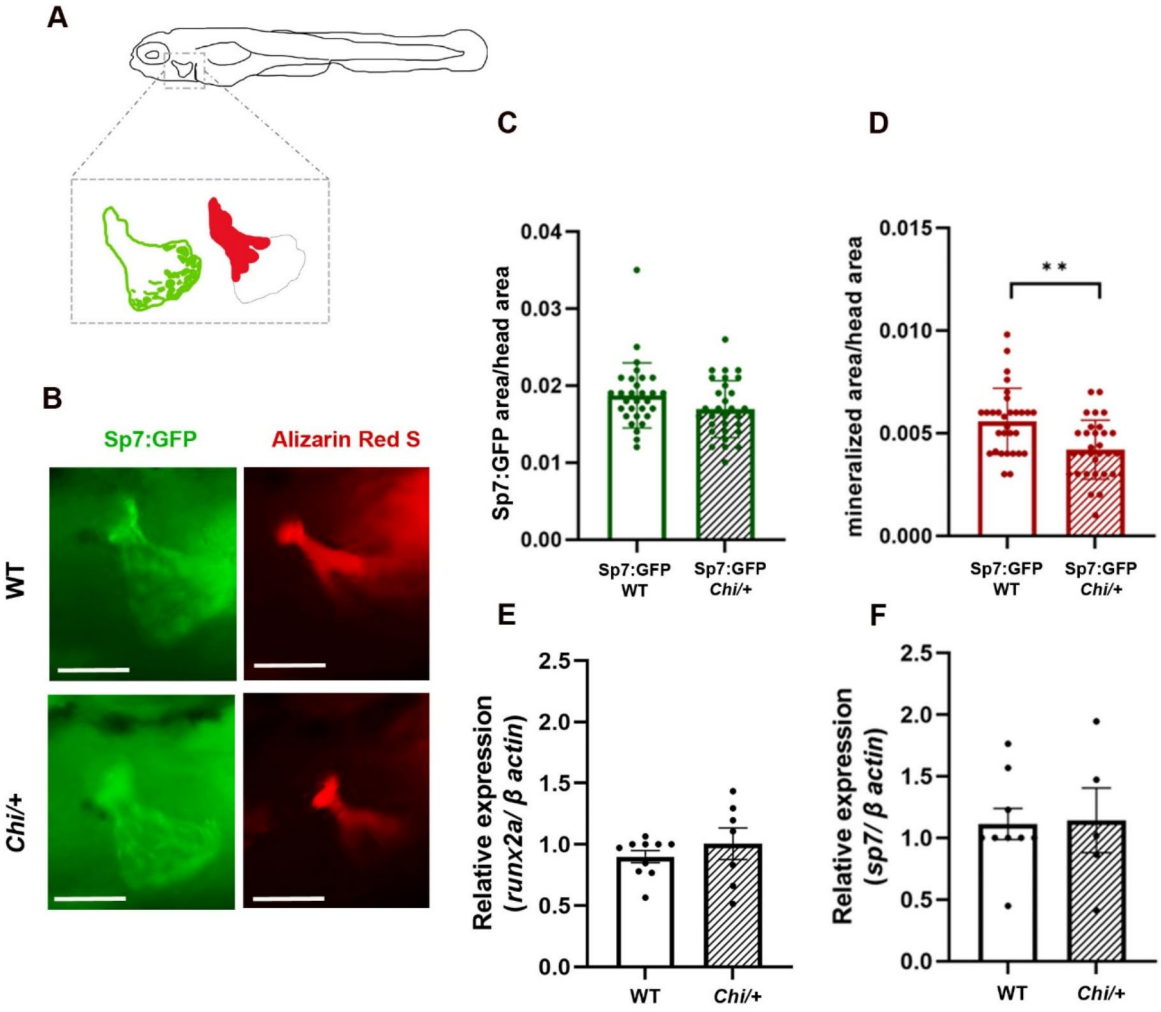

Fig. 1. Analysis of Sp7:GFP/WT and Sp7:GFP/*Chi*/+ operculum area in 6 dpf larvae. (**A**) Representative draw of 6 dpf zebrafish larvae and magnification of the operculum. Sp7:GFP osteoblast area is shown in green, while alizarin red S stained mineral in red. (**B**) Representative images of Sp7:GFP/WT and Sp7:GFP/*Chi*/+ operculum stained with alizarin red S. Scale bar: 50 µm. (**C**) Histogram showing the Sp7:GFP/WT and Sp7:GFP/*Chi*/+ operculum area delimited by osteoblasts normalized to the head area (WT: $n = 30$; *Chi*/+: $n = 31$). (**D**) Histogram showing the Sp7:GFP/WT and Sp7:GFP/*Chi*/+ mineralized operculum area normalized to the head area (WT: $n = 30$; *Chi*/+: $n = 31$). (**E**) Relative expression of *runx2a* in WT and *Chi*/+ 6 dpf larvae evaluated by RT-qPCR (WT: $n = 10$ pools; *Chi*/+: $n = 7$ pools). (**F**) Relative expression of *sp7* in WT and *Chi*/+ 6 dpf larvae evaluated by RT-qPCR (WT: $n = 9$ pools; *Chi*/+: $n = 5$ pools). Data are presented as mean ± SEM. Each point represents a single value (Wilcoxon rank-sum test; ** $p < 0.01$).

of the early osteoblastogenic markers *runx2a* and *sp7* was detectable by qPCR on RNA extracted from whole larvae (Fig. 1B, C, E, F). A significant reduction of operculum bone matrix mineralized area was evident in *Chi*/+ compared to WT, proving a delayed mineralization in this model before the 2 weeks of life, as previously reported during the model characterization (Fig. 1B, D)[12].

Our data show that, at least in the operculum, during early development *Chi*/+ preosteoblasts can normally differentiate, but the mineralization process is impaired.

Larval development in *Chi*/+ and WT is differentially affected following exposure to specific PFAS

WT and *Chi*/+ transgenic zebrafish were used to evaluate in vivo the effect of 6 days continuous exposure to three different PFAS, namely perfluorooctane sulfonate (PFOS), perfluorooctanoic acid (PFOA) and perfluorohexanoic acid (PFHxA), on larval development, early skeleton formation and mineralization. The selected doses were chosen to evaluate the potential additive effect caused by cumulative amount in the organism as a consequence of prolonged exposure, but taking advantage of the fast zebrafish organogenesis[18–20].

The standard length (SL) and the inflation of the first swim bladder lobe were evaluated as hallmarks to investigate the effect of pollutants on development in 6 dpf WT and *Chi*/+ zebrafish (Fig. 2A i, ii). To this aim, larvae were incubated from 1 to 6 dpf with the three different PFAS. PFOS significantly reduced SL in WT exposed to 1.5 and to 3 mg/L doses and in *Chi*/+ exposed to 3.0 mg/L compared to the non-exposed (indicated as controls from now on). PFOA did not affect either WT or *Chi*/+ 6 dpf SL at any of the selected doses. Similarly, no effect on both WT and *Chi*/+ larvae size was detected at 0.01 and 0.48 mg/L PFHxA concentrations, as expected based on the reported lower toxicity of PFAS with shorten carbon chains. On the other hand, a severely reduced SL was observed in both genotypes exposed to 16 mg/L compared to their respective controls, supporting potential serious toxic effect following cumulative exposures also for this molecule[31] (Fig. 2B).

The delay in swim bladder inflation was detectable only following exposure to PFOS at the higher dose (3.0 mg/L) in both WT and *Chi*/+. PFOA and PFHxA did not impair swim bladder inflation (Fig. 2C).

The higher PFOS concentration (3.0 mg/L) revealed also a strong toxicity on development, as showed by the misshaped body curvature observed in exposed larvae (Supplementary Fig. 2A).

Overall, these data indicate a negative impact of PFOS exposure on both WT and mutant zebrafish development, while no effect was detected after PFOA. PFHxA at the highest concentration impacts on both WT and *Chi*/+ zebrafish length.

Larval bone formation is differentially affected in *Chi*/+ and WT following exposure to specific PFAS

To investigate the effect of pollutants on bone cell differentiation and bone mineralization in vivo, the operculum area delimited by Sp7 positive osteoblasts (Sp7:GFP) and the mineralized area stained by alizarin red were evaluated after PFAS exposure in both transgenic lines.

PFOS significantly reduced Sp7:GFP delimited operculum area in *Chi*/+ compared to control larvae after exposure to 1.5 mg/L (Fig. 3A, B). Also PFOA reduced significantly Sp7:GFP/*Chi*/+ operculum area at the dose of 0.005 mg/L (Fig. 3A, C). No significant effect on WT Sp7:GFP delimited operculum area was observed after PFOS and PFOA exposure (Fig. 3B, C).

No effect of PFOS on mineralized operculum area was observed (Fig. 3A, D). PFOA reduced mineralization in WT at the dose of 0.005 mg/L, while the already compromised *Chi*/+ condition (Fig. 1D) was not further affected by the pollutant (Fig. 3A, E).

The Sp7 positive osteoblast operculum area was not affected after PFHxA exposure at all the three selected doses (Fig. 4A–C).

No effect on mineralization was reported upon incubation with PFHxA in any genotype (Fig. 4A, D, E). Due to the severely impaired development observed at the highest dose no further analyses were performed on PFHxA.

The highest PFOS concentration (3.0 mg/L) revealed a strong toxicity on development and on Sp7 positive osteoblast operculum area formation in both genotypes, but not on operculum mineralization (Fig. 2B, C, Supplementary Fig. 2B–D). Therefore, also this concentration was not further tested.

The reduced Sp7:GFP operculum area observed in *Chi*/+ after PFOS and PFOA exposure suggested a possible negative impact of pollutants on mutant osteoblast differentiation. Thus, the expression of the early *runx2a* and of the intermediate osteoblast marker *sp7* were evaluated on *Chi*/+ larvae exposed to PFOS 1.5 mg/L and PFOA 0.005 mg/L, the two doses that negatively impacted on Sp7:GFP operculum area formation.

PFOS and PFOA exposure did not significantly impaired *sp7* and *runx2a* expression (Fig. 5A–D).

The data reveal that PFOS and PFOA exposure compromizes preosteoblast recruitment in *Chi*/+, while only PFOA has a negative effect on WT larvae operculum mineralization. In our conditions, the short chain PFHxA did not impact on bone formation even at the highest dose.

Apoptosis is activated by PFAS exposure in WT and *Chi*/+ larvae

Nowadays, it is recognized that in many OI forms associated to the synthesis of overmodified collagen, the mutant protein is at least partially intracellularly retained causing cellular stress, autophagy and finally apoptosis activation[32–34]. In *Chi*/+ model the presence of mutant collagen accumulated in the endoplasmic reticulum was previously reported by our team[12]. To investigate if the reduced Sp7:GFP operculum area could be a consequence of preosteoblast apoptosis, the expression of pro-apoptotic and anti-apoptotic genes, namely *bida* and *bcl2a*, respectively was analysed, using RNA extracted from whole zebrafish larvae. No significant difference in apoptotic markers expression was detected (Fig. 5E-H, Supplementary Fig. 1B). Nevertheless, a slight increase in both markers was observed in *Chi*/+ exposed to 0.005 mg/L PFOA compared to control (Fig. 5F, H).

To deeper investigate if PFOA stimulated apoptosis at the level of Sp7:GFP/*Chi*/+ operculum osteoblasts whole-mount terminal dUTP nick end-labelling (TUNEL) assay was performed. The apoptotic signal was detectable inside the operculum in both control and PFOA exposed Sp7:GFP/*Chi*/+ larvae. Interestingly, the colocalization of apoptotic signal and Sp7:GFP OBs was clearly and consistently detected only in PFOA exposed *Chi*/+ larvae compared to control, supporting the activation of apoptosis in mutant immature osteoblasts (Fig. 5I, J). The variability among larvae was very high, nevertheless a slight reduced number of apoptotic fragments was detectable in WT exposed to PFOA compared to control. This data together with the upregulation of *bcl-*

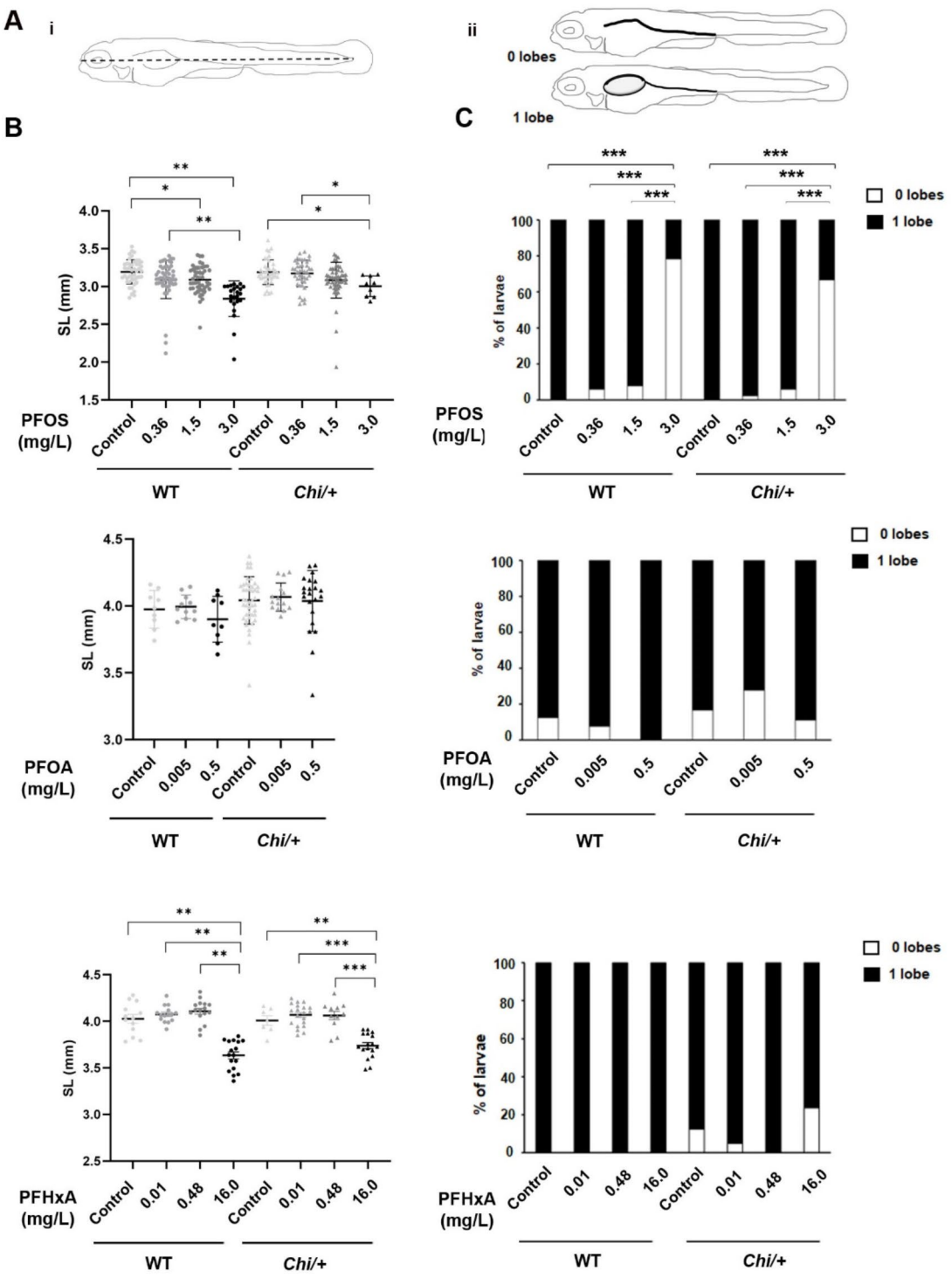

Fig. 2. Standard length and swim bladder inflation following exposure to PFAS in 6 dpf WT and *Chi*/+ zebrafish larvae. (**A**) Representative measure for standard length (SL) (i) and swim bladder inflated lobe (ii). (**B**) WT and *Chi*/+ SL after exposure to PFOS, PFOA and PFHxA. Data are presented as mean ± SD. Each point represents a single value (Kruskal-Wallis rank sum test followed by Dunnet test; * $p < 0.05$; ** $p < 0.01$; *** $p < 0.001$). (**C**) Percentage of WT and *Chi*/+ with 0 or 1 inflated swim bladder lobe after exposure to PFOS, PFOA and PFHxA. Data are expressed as percentage of larvae with 0 or 1 lobe inflated on the total number of samples analysed for each group. (PFOS, PFOA, PFHxA: WT/*Chi*/$^{+}$ $n \geq 10$, the exact numbers are reported in Supplementary Table 4) (Fisher's exact *** $p < 0.001$). Control refers to not exposed fish.

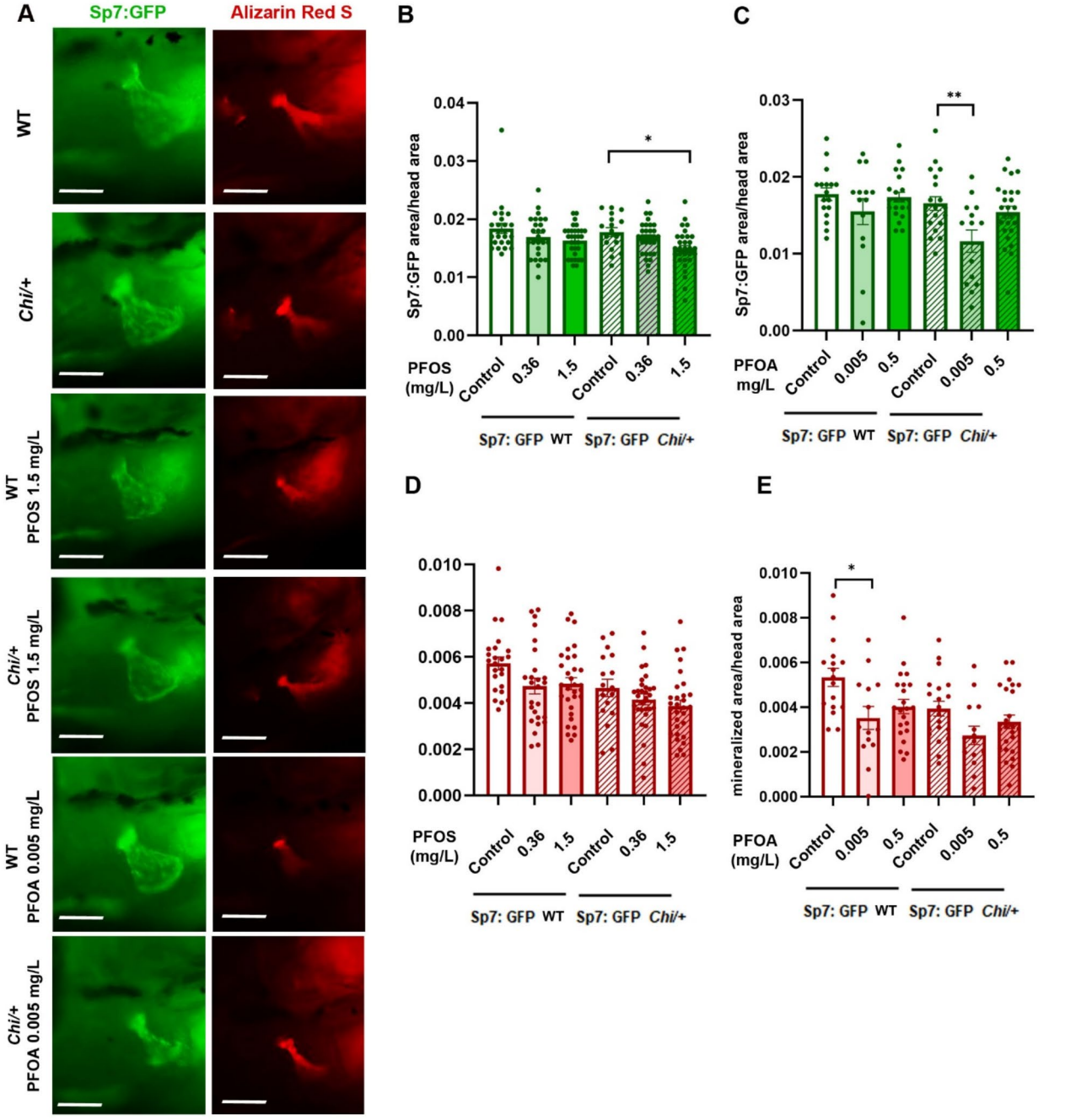

Fig. 3. Larval bone formation following exposure to PFOS and PFOA in 6 dpf WT and *Chi*/+. (**A**) Representative images of PFAS exposed Sp7:GFP/WT and Sp7:GFP/*Chi*/+ operculum stained with alizarin red S. Scale bar: 50 µm. (**B**,**C**) Histogram representing the quantification of Sp7:GFP/WT and Sp7:GFP/*Chi*/+ operculum area delimited by osteoblasts normalized to the head area following PFOS (**B**) and PFOA (**C**) exposure. (**D**,**E**) Histogram representing the quantification of Sp7:GFP/WT and Sp7:GFP/*Chi*/+ mineralized operculum area normalized to the head area following PFOS (**D**) and PFOA (**E**) exposure. (PFOS: WT/*Chi*/$^{+}$ $n \geq 17$, PFOA: WT/*Chi*/$^{+}$ $n \geq 14$, the exact numbers are reported in Supplementary Table 4). Data are presented as mean ± SEM. Each point represents a single value, (Kruskal-Wallis rank sum test; * $p < 0.05$; ** $p < 0.01$). Control refers to not exposed fish.

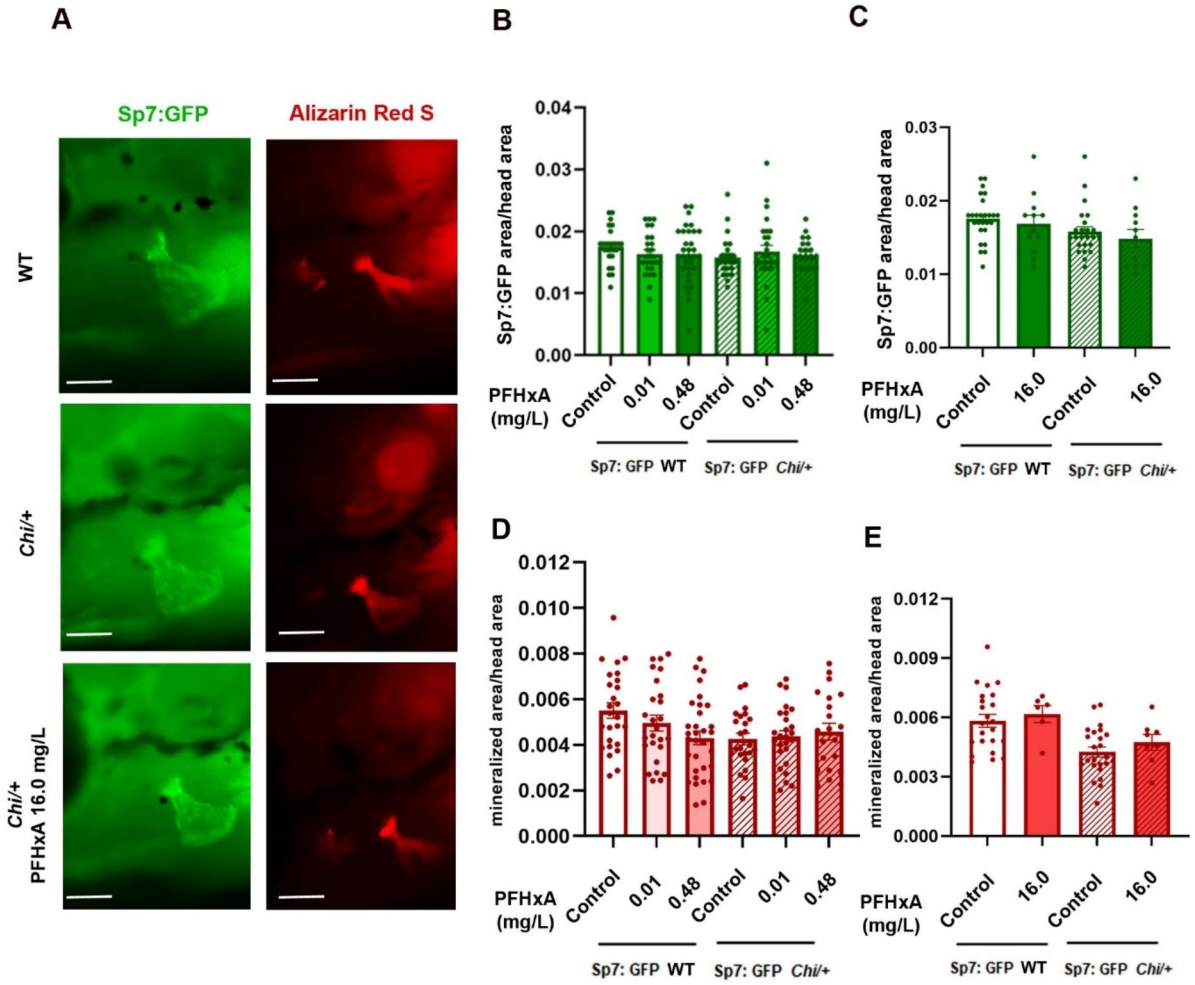

Fig. 4. Larval bone formation following exposure to PFHxA in 6 dpf WT and *Chi*/+. (**A**) Representative images of PFHxA exposed Sp7:GFP/WT and Sp7:GFP/*Chi*/+ operculum stained with alizarin red S. Scale bar: 50 µm. (**B**,**C**) PFHxA exposed Sp7:GFP/WT and Sp7:GFP/*Chi*/+ operculum area delimited by osteoblasts normalized to the head area. (**D**,**E**) PFHxA exposed Sp7:GFP/WT and Sp7:GFP/*Chi*/+ mineralized operculum area normalized to the head area. PFHxA: WT/*Chi*/$^{+}$ $n \geq 11$, the exact numbers are reported in Supplementary Table 4). Data are presented as mean ± SEM. Each point represents a single value, (Wilcoxon rank sum test). Control refers to not exposed fish.

2 expression suggest the prevalence in WT exposed to pollutant of anti-apoptotic response (Supplementary Fig. 1B, C).

Our data show an increase susceptibility to preosteoblasts apoptosis in *Chi*/+ exposed to PFOA.

Lipid distribution is affected by PFAS exposure in WT and *Chi*/+ larvae

Mesenchymal stem cells are common precursor for osteoblasts and adipocytes and a balance exists between the two cell types. A switch favouring adipocytic differentiation has been previously described in OI, associated to the altered osteoblast homeostasis due to mutant collagen intracellular accumulation[14,15]. Nevertheless, disorders of lipid metabolism have been previously associated to PFAS toxicity as revealed by a general lipidomic

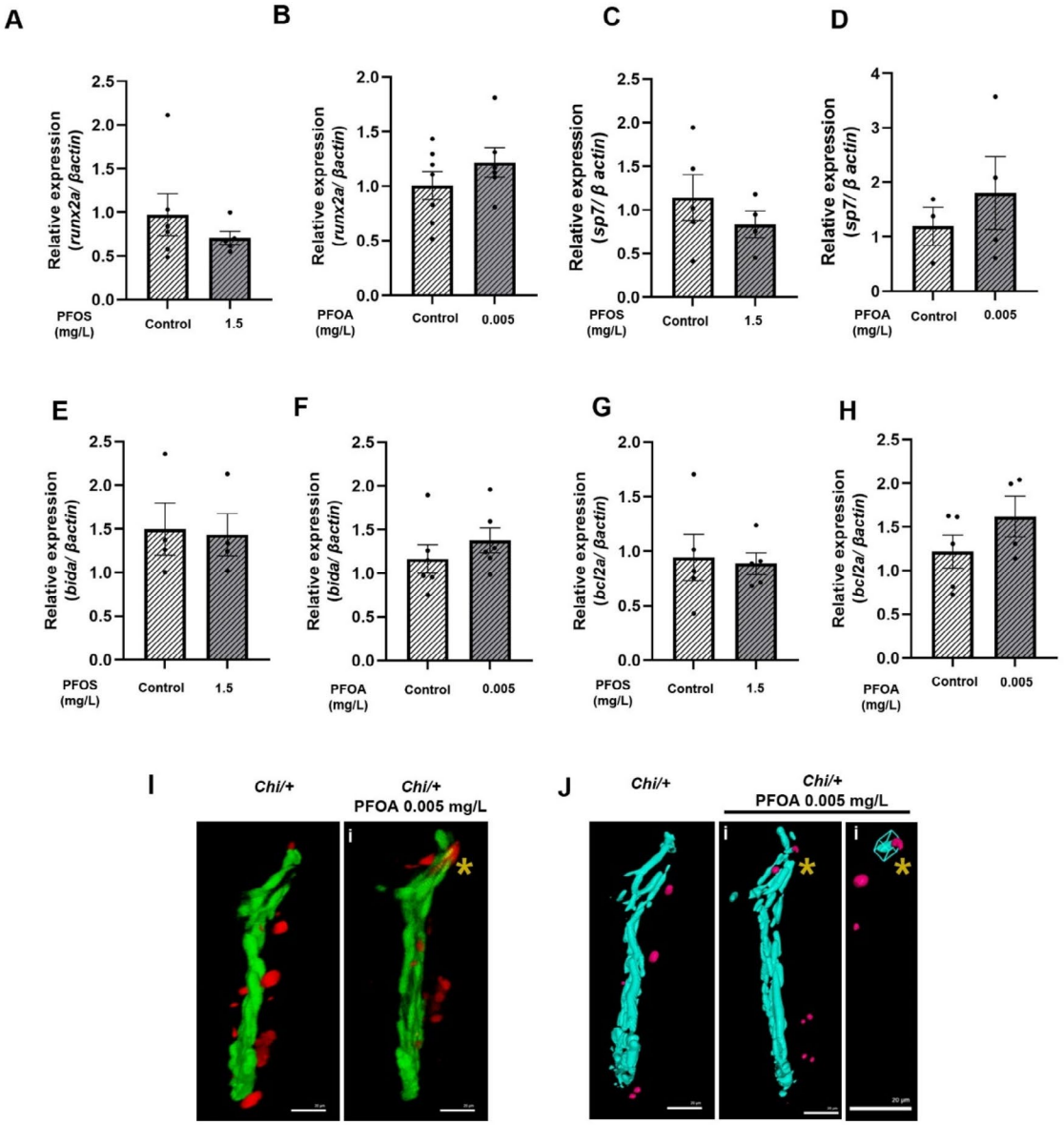

Fig. 5. Gene expression and TUNEL analysis following exposure to PFOS and PFOA in 6 dpf *Chi*/+. (**A**,**B**) Relative expression of *runx2a* in *Chi*/+ pools of larvae exposed to PFOS (**A**) and PFOA (**B**). (PFOS: *Chi*/$^{+}$ Control: $n = 6$, 1.5 mg/L: $n = 5$. PFOA: *Chi*/$^{+}$ Control: $n = 7$, 0.005 mg/L: $n = 5$. (**C**,**D**) Relative expression of *sp7* in *Chi*/+ pools of larvae exposed to PFOS (**C**) and PFOA (**D**). (PFOS: *Chi*/$^{+}$ Control: $n = 5$, 1.5 mg/L: $n = 4$. PFOA: *Chi*/$^{+}$ Control: $n = 3$, 0.005 mg/L: $n = 4$. (**E**,**F**) Relative expression of *bida* in *Chi*/+ pools of larvae exposed to PFOS (**E**) and PFOA (**F**). (PFOS: *Chi*/$^{+}$ Control: $n = 4$, 1.5 mg/L: $n = 4$. PFOA: *Chi*/$^{+}$ Control: $n = 5$, 0.005 mg/L: $n = 6$). (**G**,**H**) Relative expression of *bcl2a* in RNA extracted from *Chi*/+ pools of larvae exposed to PFOS (**G**) and PFOA (**H**). (PFOS: *Chi*/$^{+}$ Control: $n = 5$, 1.5 mg/L: $n = 5$. PFOA: *Chi*/$^{+}$ Control: $n = 5$, 0.005 mg/L: $n = 4$). Data are presented as mean ± SEM. Each point represents one pool of larvae (Wilcoxon rank sum test; not significant). Control refers to not exposed *Chi*/+ fish. (**I**) Representative 3D sagittal reconstruction of Sp7:GFP *Chi*/+ control and exposed to 0.005 mg/L PFOA larvae after TUNEL assay. Yellow asterisks indicate the colocalization of apoptotic signals in red and Sp7:GFP osteoblasts in green detected only in PFOA exposed larvae. (**J**) Representative 3D rendering of Sp7:GFP *Chi*/+ control and exposed to 0.005 mg/L PFOA after TUNEL assay. Sp7: GFP positive osteoblasts are indicated in light blue, TUNEL apoptotic signals are indicated in pink. (*Chi*/$^{+}$ Control: $n = 5$, *Chi*/$^{+}$ 0.005 mg/L: $n = 5$). Yellow asterisk indicates colocalization of apoptotic signals. Scale bar: 20 µm. Magnifications of i is shown on the right.

dysregulation associated to excessive oxidative stress damage after both PFOS and PFOA exposure in zebrafish embryos and by hepatoxicity induced by PFOS in adult zebrafish liver[35,36].

Thus, the effect of PFAS on the adipocyte distribution was evaluated in WT and *Chi*/+ before and after pollutant exposure. Since a crosstalk between bone, liver and adipose tissue exists[37,38] and the easiest site to evaluate adipocyte accumulation in 6 dpf larvae is liver, Oil red O signal was evaluated in this organ. A qualitative analysis based on the evaluation of the percentage of larvae with moderate (1), intermediate (2) or diffuse (3) spread of lipid droplets was performed (Fig. 6A). Although no interaction was observed between WT and *Chi*/+ controls, an evident increase of lipid spreading was detectable after PFOS and PFOA exposure in both genotypes (Fig. 6B, C). To investigate the effect of the mutation and of the pollutants on adipocyte

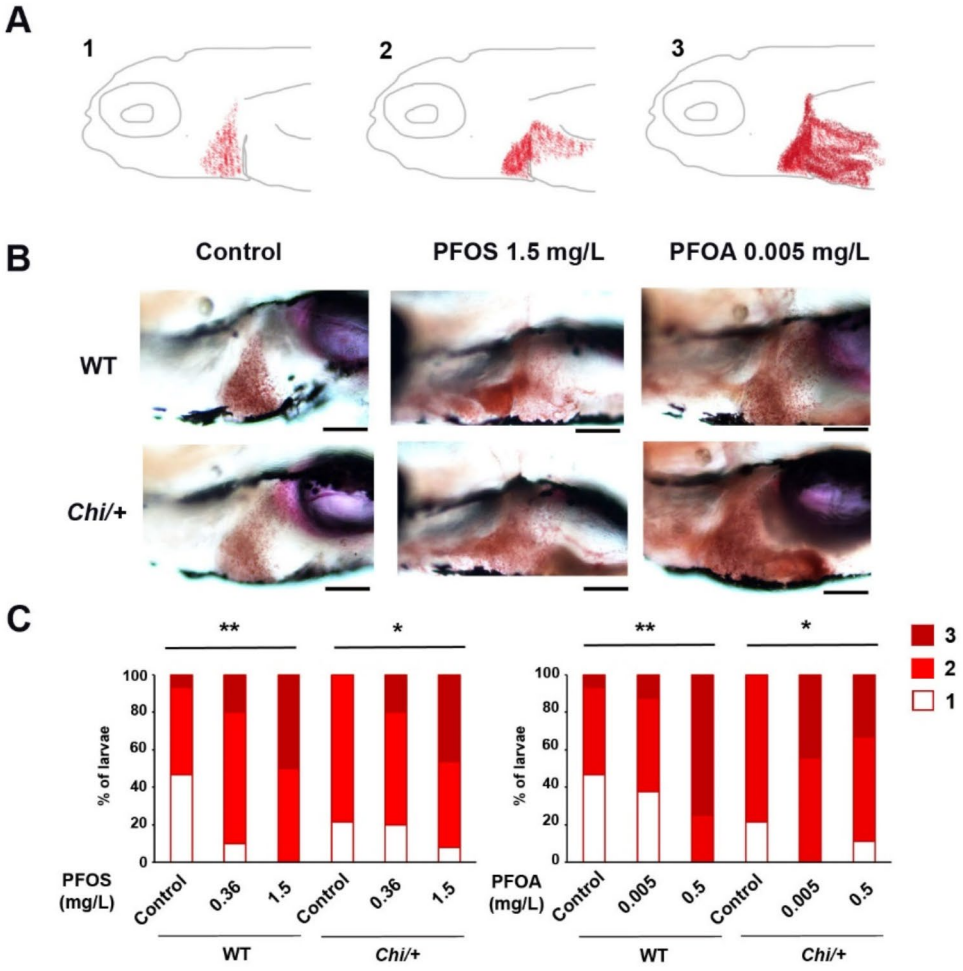

Fig. 6. Lipid distribution following exposure to PFOS and PFOA in 6 dpf WT and *Chi*/+ larvae. (**A**) Representative image of Oil red O stained lipids. The spread of lipid droplets is qualitatively represented as moderate (1), intermediate (2) or diffuse (3) according to the distribution of lipids. (**B**) Representative image of Oil red O stained lipids and in 6 dpf WT and *Chi*/+ control and exposed to pollutants. Scale Bar: 100 µm. (**C**) Percentage of fish with 1, 2 or 3 levels of lipids spread in the liver. (PFOS: WT/*Chi*/$^{+}n \geq 10$, PFOA: WT/*Chi*/$^{+}n \geq 8$, the exact numbers are reported in Supplementary Table 4). Fisher's exact test, * $p < 0.05$; ** $p < 0.01$ Control refers to not exposed fish.

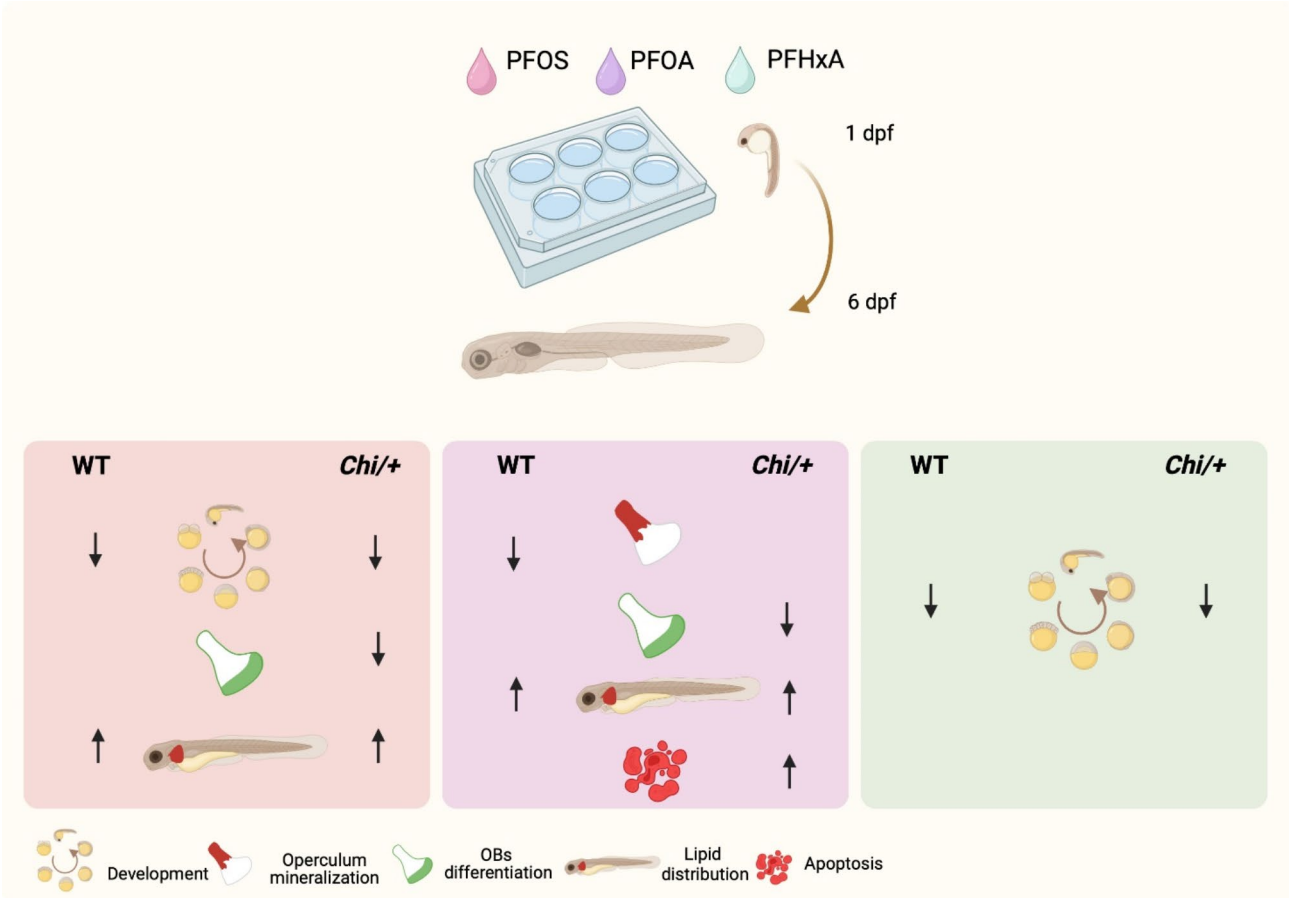

Fig. 7. Impact of PFOS, PFOA and PFHxA on development, bone cell differentiation and mineralization, apoptosis and lipid distribution in WT and *Chi*/+ larvae. Created with BioRender.com.

differentiation the expression of adipogenic markers *pparα* and *pparγ* was performed on WT and on *Chi*/+ zebrafish. The two genes encode for proteins belonging to the PPARs subfamily of ligand-activated transcription factors, critically involved in the regulation of genes related to energy homeostasis, glucose triglyceride and lipoprotein metabolism regulation, as well as de novo lipogenesis and fatty acid uptake[39]. No difference in the expression of both genes was observed (Supplementary Fig. 3A-D).

Our results support a negative effect of PFAS on hepatic lipid accumulation both in WT and in *Chi*/+ larvae in presence of normal adipocyte differentiation process.

Discussion

It is well known that environmental burdens have negative impact on human health, but what is less investigated is the severity of such effects on individuals already affected by diseases[1]. To tackle the intriguing question on the consequences of pollutants on wild-type versus brittle skeleton this study investigated the impact of three perfluorinated compounds, namely PFOS, PFOA and PFHxA on body and skeletal development in the zebrafish *Chihuahua* (*Chi*/+), a model for the rare bone disease osteogenesis imperfecta (OI) and in the WT littermates[12,40]. The transparency of zebrafish larval body and the availability of the WT and *Chi*/+ Tg(*OlSp7:nlsGFP)zf132* transgenic line expressing GFP under *osterix* promoter allowed to prove in vivo that PFAS compromise operculum preosteoblast differentiation, mineralization and survival as well as alter lipid accumulation both in control and mutant bone in dose and, for some parameters, in genotype dependent manner. Even if no interaction was present between the genotype, our data showed that in both WT and mutant larvae PFOS and the highest dose of PFHxA reduced the standard length. PFOS and PFOA incubation impaired osteoblast recruitment in the mutant, the latter also enhancing apoptosis at the level of operculum and both pollutants impaired lipid distribution in both genotype (Fig. 7).

Impact of PFAS on morphological parameters

Our results on reduced standard length and swim bladder inflation following PFOS exposure confirmed previous data showing its negative effect on 6 dpf WT zebrafish larval development, that led also to impaired swimming speed[41], and demonstrated that the pollutant is similarly affecting mutant zebrafish with brittle bones. PFOA did not impact on larval development at both concentrations tested either the mutant or control fish, likely due to the lower toxicity of compounds with carboxyl group respect to those with sulfonate group. Indeed, zebrafish

embryo deformities and reduced hatching rate were previously detected after PFOA exposure only at higher concentrations ranging from 50 to 500 mg/L[41].

Impact of PFAS on skeletal development

The main strength of our study is to provide in vivo evidence of the negative and specific effect of perfluorinated pollutants on bone cell differentiation and mineralization. Indeed, to date the available data on the effect of the perfluorinated pollutants on osteoblasts come from in vitro studies. In murine osteoblast cultures, cell viability significantly decreased after exposure to 100 µM and above of PFOA that also caused a reduced expression of osteocalcin, a late osteoblastogenic marker[42]. Moreover, PFOA up-regulated the expression of osteogenic transcription factors (*Taz*, *Runx2* and *Osterix*), type 1 collagen genes (*Col1a1* and *Col1a2*) and the cysteine-rich acidic matrix-associated gene (*Sparc*) in hMSCs-derived osteoblasts, whereas PFOS did not have any consistent effects[43].

We showed that in vivo PFOS and PFOA reduced Sp7:GFP operculum area in *Chi*/+.

On the other hand, a reduced mineralized operculum area was caused by PFOA exposure only in WT, but not in *Chi*/+, likely due to the already compromised mineralization of mutant bone that could have hidden a small negative effect following PFAS exposure. Of note, larval stage is the period during which bones start to mineralize, representing a crucial step for zebrafish bone development[9,21]. Thus, defects in bone formation at this time point could negatively impact later in development. Indeed, it was recently demonstrated that the negative correlation between PFOA and PFOS exposure and bone mineral density in children, adolescents and young adults is associated with an increased risk of bone fractures and osteoporosis in later adulthood[5,44]. Differentiation and mineralization are regulated by calcitriol, the active form of vitamin D, which blocks cell cycle and induces osteoblasts to mature. A competition of PFOA with calcitriol for vitamin D receptor at the same binding site was demonstrated in vitro as responsible for impaired differentiation and mineralization[45].

PFHxA is known as alternative to legacy PFOS and PFOA thanks to its shorter carbon chain that should reduce bioaccumulation. Previous studies showed that PFHxA is not carcinogenic, is not a selective reproductive or developmental toxicant, and does not disrupt endocrine activity. Adverse effects have been detected on human kidney, but at much higher doses than those observed for other PFAS[46]. The absence of a significant impairment in operculum development in both WT and *Chi*/+ larvae exposed to PFHxA at 16 mg/L dose highlighted the not-toxic effect of this pollutant at least on bone and in our condition.

Impact of PFAS on lipid accumulation in the liver

Zebrafish share many of the same gastrointestinal organs with humans as well as the specialized cell types involved in lipid absorption and processing such as intestinal enterocytes, fat-storing adipocytes, hepatocytes in the liver, and acinar cells of the pancreas. Thus, larvae are well suited for whole animal studies of lipid metabolism[47,48].

The increased percentage of WT and *Chi*/+ larvae with enlarged positive Oil red O signal labelling triglycerides in liver after PFOS and PFOA exposure confirmed what previously demonstrated in C57BL/6 mice where an increased liver/body ratio as well as an increased lipid deposition in the liver was described following PFOA exposure. In mice it was also proved that the pollutant led to increase *de novo* synthesis of fatty acids (FAs) and ultimately to accumulation of FAs in hepatocytes[49].

Lipidomic dysregulations upon exposure to PFOS and PFOA have also been observed in 3 dpf zebrafish embryos and associated with oxidative stress and energy metabolism malfunction, respectively[36]. Similarly to what reported in mice and in hMSCs exposed to PFOS and PFOA, no difference in the expression of *pparγ* and *pparα*, markers of lipid metabolism and energy homeostasis respectively[50], was detected in WT and *Chi*/+ exposed larvae.

Activation of apoptosis after PFOA exposure in *Chi*/+

Apoptosis is a regulatory program which has a noteworthy role during development and growth and in maintaining skeleton[51]. PFAS exposure is known to be directly correlated with the activation of apoptosis in various cell types. It was indeed recently reported that PFOA induces oocytes apoptosis[52], while both PFOS and PFOA lead to activate apoptosis in lung cancer A549 cell lines as well as in primary cultured tilapia hepatocytes[53]. Dysregulation in apoptosis has been also described in zebrafish liver cell line (ZFL) where altered expression of both pro- and anti- apoptotic proteins was detected after both PFOS and PFOA exposure[54].

Our results revealed that in vivo PFOA specifically enhances Sp7:GFP/*Chi*/+ apoptosis, as demonstrated by TUNEL assay at the level of operculum, whereas in WT the slight up-regulation of the anti-apoptotic marker *bcl2a* and the slight reduced number of apoptotic signals detected suggest the activation of defensive response.

The study presents some limitations that should be considered in data interpretation. Since the purpose was to evaluate the possible negative effect of the pollutants on skeleton we selected substances and doses on the basis of previous studies in which toxicity tests were already evaluated on zebrafish larvae[18–20]. Therefore, no specific toxicity analysis was carried out trusting previous published results. In addition, bone analyses were performed on the operculum, an intramembranous cranial bone easily detectable during early zebrafish bone formation, while gene expression was carried out on RNA extracted from the whole skeleton. Thus, the risk to have underestimated the expression results should be taken into account. Nevertheless, the combination of site-specific and more general assays could indeed provide useful information about the impact of pollutants. We are also aware that bioaccumulation requires the absorption and accumulation of contaminants over a long period of time in the body. Thus, the approach used in the present study does not really mimic bioaccumulation, even if the rapid zebrafish development somehow could represent a valid alternative to long term exposure in other models. Nevertheless, the short-term high-dose exposures used in our study mainly elucidated the impact of PFAS in the early stages of zebrafish bone development with and without an already compromised skeletal

condition. Our analysis of pollutants concentration in the collected water aimed to indirectly compare the level of absorption of these substances.

Conclusion

Our results suggest a negative impact of PFAS on *Chi*/+ operculum preosteoblast differentiation, and apoptosis susceptibility. Furthermore, the increased hepatic lipid spreading found in both WT and *Chi*/+ suggests also a dysregulation of fat metabolism, likely due to PFAS oxidative stress induction.

In conclusion, these results represent a first warning sign, supporting a negative impact of PFAS exposure on fragile skeleton.

Data availability

All data are provided within the manuscript or supplementary information files.

Received: 4 September 2024; Accepted: 7 January 2025
Published online: 17 January 2025

References

1. Panieri, E. et al. PFAS molecules: a major concern for the Human Health and the Environment. *Toxics*. **10**(2). (2022).
2. Podder, A. et al. Per and poly-fluoroalkyl substances (PFAS) as a contaminant of emerging concern in surface water: a transboundary review of their occurrences and toxicity effects. *J. Hazard. Mater.* **419**, 126361 (2021).
3. Semerád, J. et al. Screening for 32 per- and polyfluoroalkyl substances (PFAS) including GenX in sludges from 43 WWTPs located in the Czech Republic - evaluation of potential accumulation in vegetables after application of biosolids. *Chemosphere* **261**, 128018 (2020).
4. Schrenk, D. et al. Risk to human health related to the presence of perfluoroalkyl substances in food. *EFSA J.* **18** (9), e06223 (2020).
5. Cluett, R. et al. Per- and polyfluoroalkyl substance plasma concentrations and bone Mineral Density in Midchildhood: a cross-sectional study (project viva, United States). *Environ. Health Perspect.* **127** (8), 87006 (2019).
6. Pérez, F. et al. Accumulation of perfluoroalkyl substances in human tissues. *Environ. Int.* **59**, 354–362 (2013).
7. Martic, I., Jansen-Dürr, P. & Cavinato, M. Eff. Air Pollution Cell. Senescence Skin. *Aging Cells*. **11**(14). (2022).
8. Masiero, C. et al. Zebrafish Models for Skeletal and Extraskeletal Osteogenesis Imperfecta Features: Unveiling Pathophysiology and Paving the Way for Drug Discovery. *Calcif. Tissue Int.*. (2024).
9. Tonelli, F. et al. Zebrafish: a resourceful Vertebrate Model to investigate skeletal disorders. *Front. Endocrinol.*. **11**, 489 (2020).
10. Formosa, M. M., Christou, M. A. & Mäkitie, O. Bone fragility and osteoporosis in children and young adults. *J. Endocrinol. Investig.* **47** (2), 285–298 (2024).
11. Forlino, A. et al. Differential expression of both extracellular and intracellular proteins is involved in the lethal or nonlethal phenotypic variation of BrtlIV, a murine model for osteogenesis imperfecta. *Proteomics* **7** (11), 1877–1891 (2007).
12. Gioia, R. et al. The chaperone activity of 4PBA ameliorates the skeletal phenotype of Chihuahua, a zebrafish model for dominant osteogenesis imperfecta. *Hum. Mol. Genet.* **26** (15), 2897–2911 (2017).
13. Pittenger, M. F., Mosca, J. D. & McIntosh, K. R. Human mesenchymal stem cells: progenitor cells for cartilage, bone, fat and stroma. *Curr. Top. Microbiol. Immunol.* **251**, 3–11 (2000).
14. Gioia, R. et al. Impaired osteoblastogenesis in a murine model of dominant osteogenesis imperfecta: a new target for osteogenesis imperfecta pharmacological therapy. *Stem Cells*. **30** (7), 1465–1476 (2012).
15. Daponte, V. et al. Cell differentiation and matrix organization are differentially affected during bone formation in osteogenesis imperfecta zebrafish models with different genetic defects impacting collagen type I structure. *Matrix Biol.* **121**, 105–126 (2023).
16. Fisher, S., Jagadeeswaran, P. & Halpern, M. E. Radiographic analysis of zebrafish skeletal defects. *Dev. Biol.* **264** (1), 64–76 (2003).
17. Moro, E. et al. Generation and application of signaling pathway reporter lines in zebrafish. *Mol. Genet. Genom.* **288** (5–6), 231–242 (2013).
18. Mylroie, J. E. et al. Perfluorooctanesulfonic Acid-Induced toxicity on zebrafish embryos in the Presence or absence of the Chorion. *Environ. Toxicol. Chem.* **40** (3), 780–791 (2021).
19. Wang, Y. et al. Comparison of developmental toxicity induced by PFOA, HFPO-DA, and HFPO-TA in zebrafish embryos. *Chemosphere* **311** (Pt 1), 136999 (2023).
20. Guo, X. et al. Evaluation of the acute toxicity and neurodevelopmental inhibition of perfluorohexanoic acid (PFHxA) in zebrafish embryos. *Ecotoxicol. Environ. Saf.* **225**, 112733 (2021).
21. Parichy, D. M. et al. Normal table of postembryonic zebrafish development: staging by externally visible anatomy of the living fish. *Dev. Dyn.* **238** (12), 2975–3015 (2009).
22. Tonelli, F. et al. Zebrafish Tric-b is required for skeletal development and bone cells differentiation. *Front. Endocrinol.* **14**, 1002914 (2023).
23. Tonelli, F. et al. Crtap and p3h1 knock out zebrafish support defective collagen chaperoning as the cause of their osteogenesis imperfecta phenotype. *Matrix Biol.* **90**, 40–60 (2020).
24. Kimmel, C. B. et al. Modes of developmental outgrowth and shaping of a craniofacial bone in zebrafish. *PLoS One*. **5** (3), e9475 (2010).
25. Tarasco, M. et al. ZFBONE: an ImageJ toolset for semi-automatic analysis of zebrafish bone structures. *Bone* **138**, 115480 (2020).
26. Vanhauwaert, S. et al. Expressed repeat elements improve RT-qPCR normalization across a wide range of zebrafish gene expression studies. *PLoS One*. **9** (10), e109091 (2014).
27. Xia, Z. et al. Zebrafish slc30a10 deficiency revealed a novel compensatory mechanism of Atp2c1 in maintaining manganese homeostasis. *PLoS Genet.* **13** (7), e1006892 (2017).
28. Gentile, I. et al. Short-term exposure to Benzo(a)pyrene causes disruption of GnRH Network in zebrafish embryos. *Int. J. Mol. Sci.*, **24**(8). (2023).
29. Morikane, D., Zang, L. & Nishimura, N. Evaluation Percutaneous Absorption of Drug Molecules Zebrafish. *Molecules* **25**(17). (2020).
30. Tarasco, M. et al. The zebrafish operculum: a powerful system to assess osteogenic bioactivities of molecules with pharmacological and toxicological relevance. *Comp. Biochem. Physiol. C Toxicol. Pharmacol.* **197**, 45–52 (2017).
31. Borg, D. et al. Cumulative health risk assessment of 17 perfluoroalkylated and polyfluoroalkylated substances (PFASs) in the Swedish population. *Environ. Int.* **59**, 112–123 (2013).
32. Besio, R. et al. 4-PBA ameliorates cellular homeostasis in fibroblasts from osteogenesis imperfecta patients by enhancing autophagy and stimulating protein secretion. *Biochim. Biophys. Acta Mol. Basis Dis.* **1864** (5 Pt A), 1642–1652 (2018).
33. Besio, R. et al. *Cellular stress due to impairment of collagen prolyl hydroxylation complex is rescued by the chaperone 4-phenylbutyrate. Dis. Model. Mech.*, **12**(6). (2019).

34. Garibaldi, N. et al. Targeting cellular stress in vitro improves osteoblast homeostasis, matrix collagen content and mineralization in two murine models of osteogenesis imperfecta. *Matrix Biol.* **98**, 1–20 (2021).
35. Wang, Q. et al. Aberrant hepatic lipid metabolism associated with gut microbiota dysbiosis triggers hepatotoxicity of novel PFOS alternatives in adult zebrafish. *Environ. Int.* **166**, 107351 (2022).
36. Yang, Z. et al. PFAS-induced lipidomic dysregulations and their associations with developmental toxicity in zebrafish embryos. *Sci. Total Environ.* **861**, 160691 (2023).
37. Musso, G. et al. Interactions among bone, liver, and adipose tissue predisposing to diabesity and fatty liver. *Trends Mol. Med.* **19** (9), 522–535 (2013).
38. Labayen, I. et al. Liver Fat, Bone Marrow adipose tissue, and bone Mineral density in children with overweight. *J. Clin. Endocrinol. Metab.* **109** (1), e253–e258 (2023).
39. Han, L. et al. PPARs: regulators of metabolism and as therapeutic targets in cardiovascular disease. Part II: PPAR-β/δ and PPAR-γ. *Future Cardiol.* **13** (3), 279–296 (2017).
40. Fiedler, I. A. K. et al. Severely impaired bone material quality in Chihuahua zebrafish resembles classical Dominant Human Osteogenesis Imperfecta. *J. Bone Min. Res.* **33** (8), 1489–1499 (2018).
41. Hagenaars, A. et al. PFOS affects posterior swim bladder chamber inflation and swimming performance of zebrafish larvae. *Aquat. Toxicol.* **157**, 225–235 (2014).
42. Koskela, A. et al. Effects of developmental exposure to perfluorooctanoic acid (PFOA) on long bone morphology and bone cell differentiation. *Toxicol. Appl. Pharmacol.* **301**, 14–21 (2016).
43. Liu, S. et al. Environmental and human relevant PFOS and PFOA doses alter human mesenchymal stem cell self-renewal, adipogenesis and osteogenesis. *Ecotoxicol. Environ. Saf.* **169**, 564–572 (2019).
44. Beglarian, E. et al. Exposure to perfluoroalkyl substances and longitudinal changes in bone mineral density in adolescents and young adults: a multi-cohort study. *Environ. Res.* **244**, 117611 (2024).
45. Di Nisio, A. et al. Endocrine disruption of vitamin D activity by perfluoro-octanoic acid (PFOA). *Sci. Rep.* **10** (1), 16789 (2020).
46. Luz, A. L. et al. Perfluorohexanoic acid toxicity, part I: development of a chronic human health toxicity value for use in risk assessment. *Regul. Toxicol. Pharmacol.* **103**, 41–55 (2019).
47. Anderson, J. L., Carten, J. D. & Farber, S. A. Zebrafish lipid metabolism: from mediating early patterning to the metabolism of dietary fat and cholesterol. *Methods Cell. Biol.* **101**, 111–141 (2011).
48. Wallace, K. N. et al. Intestinal growth and differentiation in zebrafish. *Mech. Dev.* **122** (2), 157–173 (2005).
49. Weng, Z. et al. Autophagy mediates perfluorooctanoic acid-induced lipid metabolism disorder and NLRP3 inflammasome activation in hepatocytes. *Environ. Pollut.* **267**, 115655 (2020).
50. Tyagi, S. et al. The peroxisome proliferator-activated receptor: a family of nuclear receptors role in various diseases. *J. Adv. Pharm. Technol. Res.* **2** (4), 236–240 (2011).
51. Mollazadeh, S., Fazly Bazzaz, B. S. & Kerachian, M. A. Role of apoptosis in pathogenesis and treatment of bone-related diseases. *J. Orthop. Surg. Res.* **10**, 15 (2015).
52. López-Arellano, P. et al. Perfluorooctanoic acid disrupts gap junction intercellular communication and induces reactive oxygen species formation and apoptosis in mouse ovaries. *Environ. Toxicol.* **34** (1), 92–98 (2019).
53. Liu, C. et al. Induction of oxidative stress and apoptosis by PFOS and PFOA in primary cultured hepatocytes of freshwater tilapia (Oreochromis niloticus). *Aquat. Toxicol.* **82** (2), 135–143 (2007).
54. Cui, Y. et al. Investigation of the effects of Perfluorooctanoic Acid (PFOA) and Perfluorooctane Sulfonate (PFOS) on apoptosis and cell cycle in a zebrafish (Danio rerio) Liver Cell line. *Int. J. Environ. Res. Public Health*. **12** (12), 15673–15682 (2015).

Acknowledgements

We thank the animal facility "Centro di servizio per la gestione unificata delle attività di stabulazione e di radiobiologia" of the University of Pavia, Pavia, Italy, for animal care. We thank Eleonora Riva for help with initial experiments. We acknowledge Dr.Amanda Oldani and Dr.Patrizia Vaghi "Centro Grandi Strumenti", University of Pavia, Italy, for providing confocal and widefield microscopy support.

Author contributions

Francesca Tonelli: Conceptualization, Methodology, Software, Validation, Data curation, Writing-original draft. Cecilia Masiero and Carla Aresi: Methodology, Writing-review & editing. Simona Villani, Camilla Torriani: statistical analysis of the data. Guido Premoli: Methodology, Validation. Antonio Rossi: Writing- review & editing. Antonella Forlino: Conceptualization, Supervision, Writing-original draft, Writing-review & editing, Founding acquisition. All the authors have read and approved the manuscript.

Funding

This work was supported by Italian Ministry of Education, University and Research (MIUR) [Dipartimenti di Eccellenza (2023–2027)] to AF; by Regione Lombardia, "regionallawn°9/2020, resolutionn°3776/202000 to AF; PON-React-EU Research and Innovation 2014–2020 art 34, paragraph 3 a), law 30th December 2010, n.240 and s.m.i and D.M. 10th August 2021 n. 1062 to FT.

Declarations

Competing interests

The authors declare no competing interests.

Additional information

Supplementary Information The online version contains supplementary material available at https://doi.org/10.1038/s41598-025-85967-3.

Correspondence and requests for materials should be addressed to A.F.